

Design and Fabrication of an Autonomous Solar Powered Airship

By

Mitchell Van Lee, Jr.

Submitted in partial fulfillment  
of the requirements for  
Honors in the Department of Mechanical Engineering

UNION COLLEGE

June, 2011

## ABSTRACT

LEE, MITCHELL      Design and Fabrication of an Autonomous Solar Powered Airship. Department of Mechanical Engineering, June 2011.

ADVISOR: David Hodgson, PhD

The purpose of the project was to design and build a prototype small scale photovoltaic (PV) powered autonomous airship. The principle reason for the construction of the unmanned airship was to investigate the possibility of using self-guided, lighter-than-air aircraft as an alternative to earth observational satellites for the purposes of terrain mapping and imaging. The necessary electrical energy was produced by single crystal photovoltaic solar cells. The airship was designed to carry an onboard battery in order to provide power generation in the case of intermittent cloud coverage. It was also designed to interface with an Arduino prototyping board which would supply the artificial intelligence necessary for self navigation. Radio controlled capabilities were included in case of malfunction or emergency.

The airship design process was assisted by computational design tools written in MATLAB language. These scripts made it possible to define the geometry, lift, aerodynamic drag, and envelope (balloon) membrane stresses of potential airship designs. The results from the computational programs, and additional calculations, were used to create a complete CAD rendering of the airship using SolidWorks. All airship components were fabricated and assembled, except for the envelope. Preliminary testing results are included, as well as, recommendations for design improvements.

## Contents

1 Introduction.....	1
1.1 Project .....	1
1.2 Design Criterion.....	2
2 Creation of Design Assistance Tools.....	3
2.1 Geometry .....	3
2.2 Aerodynamic Drag.....	5
2.3 Envelope Membrane Stresses .....	6
2.3.1 Method 1 .....	6
2.3.2 Method 2 .....	7
2.4 Static Lift .....	10
3 Design and Materials Selection Process .....	11
3.1 Overall Concerns .....	12
3.2 Envelope .....	12
3.2.1 Geometry.....	12
3.2.2 Aerodynamic Analysis.....	13
3.2.3 Stress Analysis .....	13
3.2.4 Envelope Fabrication Methodology.....	14
3.2.5 Lift Analysis .....	16
3.3 Propulsion and Navigation.....	17
3.3.1 Introduction to Propulsion and Navigation System.....	17
3.3.2 Motor and Ducted Fans .....	17
3.3.3 Speed Controller .....	18
3.3.4 Servo .....	20
3.3.5 Receiver and Transmitter.....	20
3.3.6 Photovoltaic Cells.....	20
3.3.7 Battery and Charge Controller .....	21
3.3.8 Summary of Propulsion and Navigation Systems .....	22
3.4 Rigid Structural Components.....	23
3.4.1 PV Cell Backing .....	23
3.4.2 Fins .....	24
3.4.3 Gondola.....	25
3.5 Fan and Axle Assembly .....	28

4 Testing and Results.....	29
4.1 Envelope .....	29
4.2 Propulsion and Power Generation.....	31
4.2.1 <i>Propulsion and Navigation</i> .....	31
4.2.2 <i>Photovoltaic Charging System</i> .....	32
4.3 Weight Analysis.....	33
5 References.....	34
6 Appendix.....	35
6.1 Geometry Derivations.....	35
6.2 Detailed Circuit Diagram.....	37
6.3 Engineering Drawings .....	37

# **1 Introduction**

## **1.1 Project**

The purpose of the project was to design and build a prototype small scale photovoltaic (PV) powered autonomous airship. The principle reason for the construction of the unmanned airship was to investigate the possibility of using self-guided, lighter-than-air aircraft as an alternative to earth observational satellites for the purposes of terrain mapping and imaging. The use of earth observational satellites has several inherent drawbacks. Particular disadvantages include prohibitive cost, difficulty of maintenance, and the necessary tradeoff between small observation range (geostationary satellites), or infrequent image rate of a particular location (polar orbiting). The use of airships for terrain imaging would be considerably less expensive than satellite launching. Combining the necessary artificial intelligence and photovoltaic cells to generate electrical propulsion would remove the necessity to land for the purposes of re-staffing and refueling. Furthermore, the use of airships would allow for continually monitoring of a specific region for a designated time frame. In addition, when the monitoring project had been completed the airship could be moved to a new location of interest.

The end goal was to create an electrically propelled helium-filled airship which could capture composite aerial images of outdoor events, such as ReUnion Weekend, at Union College during spring term 2011. It was desired for the device to have the artificial intelligence necessary for self navigation through the use of an Arduino prototyping board. It was to also have radio controlled override capabilities to be used in case of malfunction or emergency. The electrical energy was produced by polycrystalline photovoltaic solar cells. It was also to carry an onboard battery with charge controller in order to provide power generation in the case of intermittent cloud coverage.

It should be noted that the project was not full completed. Thus, the results section presented is limited. Nevertheless, recommendations are made on how to solve the remaining design and fabrication challenges.

## **1.2 Design Criterion**

In order for the finalized design to be considered a success, it must meet the following criteria:

1. Be capable of lift as a result of buoyancy without relying on aerodynamic surfaces
2. Capable of capturing aerial images
3. Capable of self-navigation with radio controlled (RC) override.
4. Capable of indefinite powered flight, as long as there is sunlight with minimal cloud coverage
5. Reach a top airspeed of 5 m/s
6. Cost less than \$1000 to design and construct

The first four design criteria are to serve as a “proof of concept” for photovoltaic airship geostationary earth observation. While a full size airship would be capable of sustained nighttime flight, this feature is not achievable on a small scale. As will be further explained later in the report, lift does not scale proportionately with airship size. As a result, adding enough batteries for night propulsion would make the airship too heavy for lift off. Nevertheless, the airship will have batteries for storing photovoltaic generated electricity. This will allow for pulses of power consumption greater than PV generation. This will also allow for flight during brief periods of cloud coverage. Criterion 5 was selected so that the airship would be capable of traveling twice the wind speed on a calm day in Schenectady, New York. Finally, the airship must cost less than \$1,000 because that is the maximum funding Union College’s Internal Educational Fund will provide for student projects.

## 2 Creation of Design Assistance Tools

In order to simplify the design process, a series of MATLAB scripts were written as design tools. These scripts make it possible to define the geometry, lift, aerodynamic drag, and envelope (balloon) membrane stresses of potential airship designs.

### 2.1 Geometry

In order to design the airship, it was necessary to mathematically define the shape of the envelope. It was discovered that most envelope shapes can be made by joining two half prolate spheroids which have the same maximum radius. This is illustrated in Figure 1.

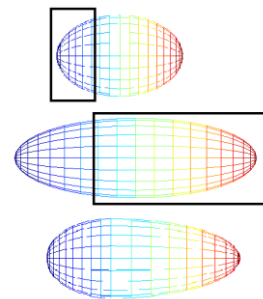
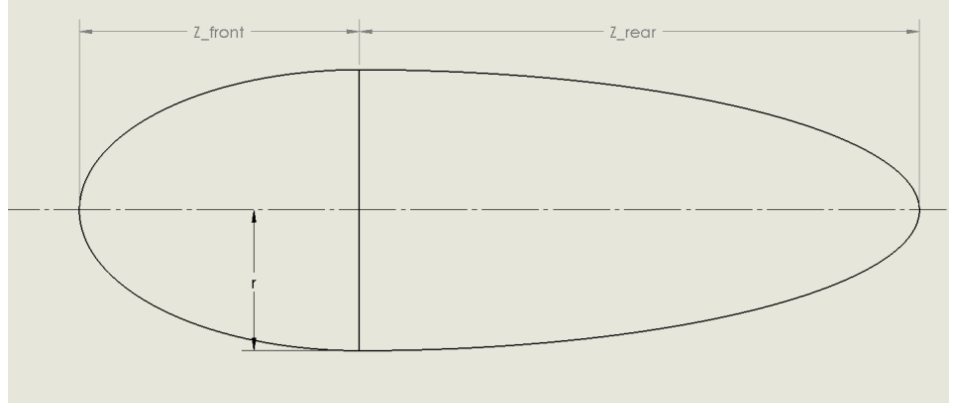


**Figure 1: Envelope Shape**

The MATLAB script which will fully define an envelope shape requires three basic inputs. The three inputs are:

1. The volume,  $V$ , of the balloon,
2.  $c_1$ , the ratio of the length of the balloon in front of the largest cross-section to the maximum radius
3.  $c_2$ , the ratio of the length of the balloon behind the largest cross-section to the length of the balloon in front of the largest cross-section.

Figure 2 illustrates inputs two and three.



$$\text{input 2} = c_1 = \frac{z_{front}}{r}; \text{input 3} = c_2 = \frac{z_{front}}{z_{rear}}$$

**Figure 2: Shape Inputs**

The maximum radius of the envelope,  $r$ , is calculated using Equation 1 printed below.

$$r = \left[ \frac{3V}{2\pi c_1 + c_2 c_3} \right]^{\frac{1}{3}} \quad (1)$$

The length of the envelope in front of the maximum radius,  $z_{front}$ , was calculated using Equation 2, and the length of the envelope behind the maximum radius,  $z_{rear}$ , was calculated using Equation 3.

$$z_{front} = r c_1 \quad (2)$$

$$z_{rear} = z_{front} c_2 = r c_1 c_2 \quad (3)$$

The surface area of the envelope,  $A$ , was calculated using Equation 4.

$$A = \pi \left( 2(r^2) + \frac{r(z_{front})(\alpha_{front})}{\sin \alpha_{front}} + \frac{r(z_{rear})(\alpha_{rear})}{\sin \alpha_{rear}} \right) \quad (4)$$

$$\text{where: } \alpha_{front} = \cos^{-1} \left( \frac{r}{z_{front}} \right)$$

$$\alpha_{rear} = \cos^{-1} \left( \frac{r}{z_{rear}} \right)$$



A brief derivation of equations 1 through 4 can be seen in the Appendix, Section 6.1.

## **2.2 Aerodynamic Drag**

The MATLAB script which determines the drag force resisting forward motion,  $F_D$ , draws upon the data in the geometry program. The additional inputs needed are:

1.  $\rho_a$ , the density of the ambient air
2.  $\mu_a$ , the viscosity of the ambient air
3.  $v_a$ , the airspeed of the airship

The Reynolds number,  $Re$ , is needed to calculate the drag force on the airship. It is calculated using Equation 5 printed below.

$$Re = \frac{\rho_a v_a l}{\mu_a} \quad (5)$$

where:  $l = z_{front} + z_{rear}$

The drag coefficient,  $C_D$ , of an airship envelope is calculated using Equation 6 (Gillett, & Khoury, 2004, p.32).

$$C_D = \frac{\left[ 0.172 \left( \frac{l}{2r} \right)^{\frac{1}{3}} + 0.252 \left( \frac{2r}{l} \right)^{1.2} + 1.032 \left( \frac{2r}{l} \right)^{2.7} \right]}{Re^{\frac{1}{6}}} \quad (6)$$

Equation 6 is an empirical formula developed by S.F. Hoerner for airships with Reynolds numbers greater than  $5 \times 10^6$ .  $F_D$  is calculated using Equation 7 (Gillett, & Khoury, 2004, p.28).

$$F_D = \frac{C_D \rho_a v_a^2 V^{\frac{2}{3}}}{2} \quad (7)$$

The drag force calculated using Equation 7 only includes the drag which results from the envelope. According to *Airship Design*, the bare hull accounts for approximately 50 percent of

the entire drag (Gillett, & Khoury, 2004, p.34). As a result, the MATLAB script reports the total drag force on an airship to be  $2F_D$ . This program only provides a rough estimate for the aerodynamic forces acting on an airship. In order to have more accurate results, it will be necessary to conduct a wind tunnel or Computation Fluid Dynamics analysis.

## **2.3 Envelope Membrane Stresses**

### **2.3.1 Method 1**

In order to achieve lift, it is desirable to make the envelope fabric as thin, and light, as possible. Being a non-ridged design, the airship will maintain its shape solely by means of the internal pressure within its envelope. As a result, it is important to ensure that the tensile stresses exerted on the envelope as a result of inner pressure do not cause structural failure. To provide verification of results, the stresses on the fabric can be calculated using two different MATLAB scripts, each using a different empirical methodology.

The first methodology is based on the Federal Aviation Administration, FAA, equation for the maximum bending moment in flight,  $M$ , and was developed within *Airship Technology* (Gillett, & Khoury, 2004, p.181). The FAA formula is printed below as Equation 8.

$$M = 0.029 \left[ \left( 1 + \frac{l}{2r} - 4 \right) (0.5624l^{0.02} - 0.5) \right] \rho_a u v_a V l^{0.25} \quad (8)$$

where:  $l$  = length of airship (ft)

$r$  = maximum envelope radius (ft)

$\rho_a$  = ambient air density  $\left( \frac{\text{slugs}}{\text{ft}^3} \right)$

$u$  = gust velocity  $\left( \frac{\text{ft}}{\text{s}} \right)$

$v_a$  = airship airspeed  $\left( \frac{\text{ft}}{\text{s}} \right)$

$V$  = total envelope volume (ft<sup>3</sup>)

The script calculates the minimum superpressure,  $P_{min}$ , needed to keep the airship rigid using Equation 9 printed below. The superpressure is the pressure of the internal gas at the lowest point in the envelope. In Equation 9,  $T$  is the thrust applied by an airship's motors and is equal to the drag force,  $F_D$ , for an airship at constant velocity.

$$P_{min} = \frac{1}{\pi r^3} (2M + T) \quad (9)$$

Recognizing that in practice the airship will be over pressurized, the actual superpressure,  $P_{act}$ , was estimated to be  $1.5P_{min}$ . The maximum longitudinal stress,  $\sigma_{Lmax}$ , in the envelope is found using Equation 10.

$$\sigma_{Lmax} = -\frac{Mr}{I} - \frac{(T + P_{act}(\pi r^2))}{2\pi r t} \quad (10)$$

In Equation 10,  $t$  is the fabric thickness, and  $I$  is the area moment of inertia of the cross section with the largest radius. For a circular ring with a small hoop thickness,  $I$  can be found using Equation 11.

$$I = \pi t r^3 \quad (11)$$

The maximum hoop stress,  $\sigma_{Hmax}$ , in the envelope is found using Equation 12.

$$\sigma_{Hmax} = \frac{P_{act} r}{t} \quad (12)$$

### 2.3.2 Method 2

The second MATLAB script for determining the fabric stresses draws from empirical analysis in *Airship Design* (Burgess, 2004, p.111-123). This method makes it possible to determine the envelope stresses at all longitudinal cross-sections of an airship. Unlike the first method which relies on the FAA bending moment formula, it does not account for loads attributed to propeller thrust. Burgess' method is based on the principle that the ordinary formula for normal stresses in a homogeneous beam under a shear force can be applied to an airship envelope. The equation for normal stress,  $\sigma$ , is printed below as Equation 13.

$$\sigma = \frac{Mc}{I} \quad (13)$$

In Equation 13,  $c$  is the maximum distance from the neutral axis.  $I$  is the area moment of inertia of a given cross-section. The cross-section is considered to be an infinitely thin ring.  $I$  is in the units of  $\text{m}^3$  instead of  $\text{m}^4$ . This is because it is customary to express stress in an infinitely thin ring using the units of  $\text{N/m}$  instead of  $\text{N/m}^2$ . The bending moment,  $M$ , is composed of three parts. The first part results from the uneven distribution of vertical weight and buoyancy forces along the length of the envelope. The second results because the gas pressure at the top of the envelope is greater than at the bottom. This causes the lengthwise tension of the envelope to be greater at its top than at its bottom. The third moment causing factor is the longitudinal components of the gondola suspension. These forces are below the neutral axis and produce bending moments comparable to those caused by an offset load on a column.

Using Burgess' method of analysis, the gas pressure bending moment and the longitudinal force for a given cross-section are found using equations 14 and 15 respectively. The MATLAB script found the bending moments and longitudinal forces at 1 mm intervals down the length of the airship.

$$M = \frac{kr^4}{24} [3\pi - 6\alpha + (2 \sin^2 \alpha - 5) \sin 2\alpha] \quad (14)$$

$$F = \pi P_{act} r^2 + \frac{kr^3}{6} [4\cos^3 \alpha - (3\pi - 6\alpha - 3 \sin \alpha) \sin \alpha] \quad (15)$$

To see derivations of equations 14 and 15 refer to *Airship Design* by Charles P. Burgess (p.117-118). In equations 14 and 15,  $k$  is the unit lift of the internal gas, which is equal to the difference between the weight of the lifting gas and weight of the air per unit volume. Figure 3 below, represents a cross-section of an airship envelope. In the figure,  $r\sin(\alpha)$  marks the level down to which the envelope is filled with helium. When  $\alpha$  is equal to  $-\pi/2$ , the envelope is completely filled with helium.

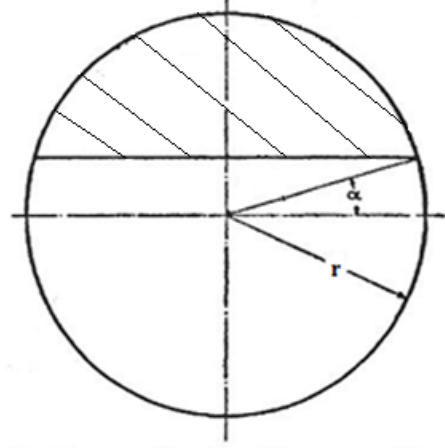


**Figure 3: Burgess Moment and Force Geometry**

The longitudinal stress,  $T_l$ , for an element of the airship envelope is given by Equation 16. In the equation,  $r$  is the radius of the circular cross section to which the element belongs.

$$T_l = \frac{F}{2\pi r} + \frac{Mr}{I} \quad (16)$$

The radial or transverse stress,  $T_t$ , is solved for through the use of Equation 17. In the equation,  $r_l$  is the longitudinal radius of curvature of the envelope for a given cross-section.

$$P = \frac{T_l}{r_l} + \frac{T_t}{r} \rightarrow T_t = Pr - \frac{T_l r}{r_l} \quad (17)$$

Both the longitudinal and transverse stresses are found in the MATLAB script at 1 mm intervals along the entire length of the envelope. Also in Equation 17,  $P$  is the pressure acting on the element of interest. The pressure of the element is found using Equation 18. In Equation 18,  $P_o$  is the pressure at the bottom of the envelope, also known as the superpressure. In Equation 18,  $h$  is the distance that the element is above the bottom of the envelope.

$$P = P_o + 2kh \quad (18)$$

$P$  is greatest at the top of a circular-section, when  $h$  is equal to  $2r$ . Because  $T_l$  is greatest when  $P$  is greatest, the MATLAB script only calculates the transverse stresses along the top ridge of the airship envelope.

In order to express the stresses in the envelope in pascals, they must be divided by the skin thickness  $t$ . Once expressed in conventional units, the longitudinal and hoops stresses are notated by using  $\sigma_L$  and  $\sigma_H$ , respectively. This is the same notation used in the first method which is based on the FAA formula.

## **2.4 Static Lift**

The first step the MATLAB script makes in calculating the airship's lift is to find its buoyancy. This is also known as an airship's gross static lift,  $L_g$ , and is calculated using Equation 19. Note that the unit of lift is kg. In the equation,  $\rho_a$  is the density of the ambient air. Currently,  $\rho_a$  is programmed to be  $1.225 \text{ kg/m}^3$ , the density at 101 kPa and 288 K.

$$L_g = V\rho_a \quad (19)$$

Next, it is necessary to determine the density of the gas inside of the airship. The first step in doing this is to determine the density of the gas assuming it to be pure helium. As seen in Equation 20, the density of the helium,  $\rho_{He}$ , can be found using the ideal gas law.

$$P = \rho_{He}R_{He}T \rightarrow \rho_{He} = \frac{P}{R_{He}T} \quad (20)$$

In Equation 20,  $R_{He}$  is the specific gas constant of helium and is equal to 2.0771 kJ/kg·K.  $T$  is the temperature of the helium, and the default temperature is 288 K. The pressure,  $P$ , was chosen as the actual pressure,  $P_{act}$ , from the first envelope membrane stress program. Impurities in the lifting gas are accounted for using Equation 21. In the equation,  $\rho_g$  is the density of the gas mixture and  $k_{He}$  is the percent helium of the gas mixture. The program default value of  $k_{He}$  is 0.98.

$$\rho_g = \rho_{He}k_{He} + \rho_a(1 - k_{He}) \quad (21)$$

The MATLAB script requires the volume of the envelope skin,  $V_s$ , in order to calculate the skin's weight. The volume is determined using Equation 22. In the equation,  $A$  is surface area of the envelope and  $t_s$  is the envelope skin thickness.

$$V_s = A_s t_s \quad (22)$$

As seen in Equation 23, the mass of the skin,  $m_s$ , is equal to the density of the skin multiplied by its volume.

$$m_s = \rho_s V_s \quad (23)$$

The net lift,  $L_n$ , of the airship is the gross static lift minus the mass of the enclosed gases, the mass of the envelope skin, and the mass of all other components,  $m_{other}$ .  $L_n$  is found using Equation 24.

$$L_n = V(\rho_a - \rho_g) - m_s - m_{other} \quad (24)$$

### **3 Design and Materials Selection Process**

All of the airship's primary systems are interrelated. Because the modification or addition of components has a profound impact on other, sometimes seemingly unrelated systems, the design process was cyclical. A simplified version of the iterative design process is summarized by Figure 4. The author believes that rehashing multiple iterative cycles is not necessary and will be uninteresting to the reader. Instead, the author will describe final design and component decisions, as well as, the thought processes and factors which directly led to those decisions.

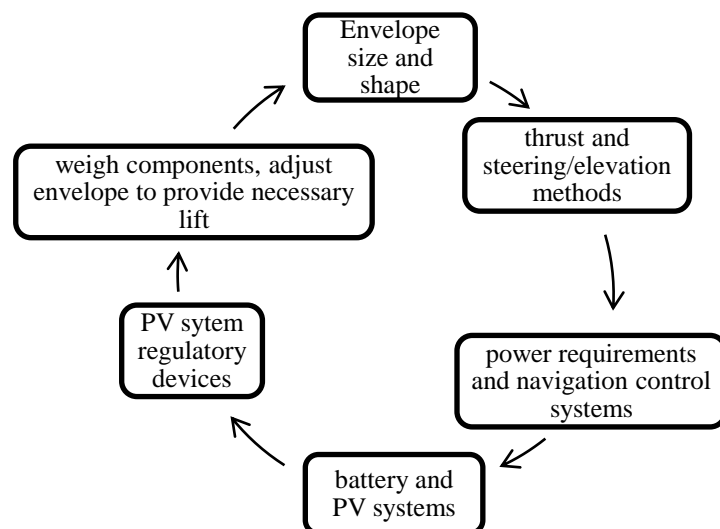


**Figure 4: Design Process**

### 3.1 Overall Concerns

As stated in section 1.2, the design must be at least neutrally buoyant, have a maximum flight speed of at least 5.00 m/s, and have an unlimited flight time given appropriate lighting conditions. The larger the airship design, the more easily these design criteria are met. When increasing the size of an envelope with constant proportions, the shape's volume increases more quickly than its surface area. Assuming constant skin thickness, the buoyancy is directly related to the airship volume, and the skin mass is directly related to the surface area. As a result, the net lift of the airship will increase disproportionately with size, and larger airships can accommodate disproportionately larger motors and batteries than smaller airships. For cost and fabrication reasons, it was desirable to make the airship as small as possible while still reaching the design objectives outlined within the introduction

### 3.2 Envelope

#### 3.2.1 Geometry

To be reminded of the airship geometry variables, refer back to Figure 2 in Section 1.2. For the finalized envelope geometry it was decided that the volume,  $V$  would be equal to  $5 \text{ m}^3$ . It was also decided that  $z_{front}/r$  was equal to 2 and  $z_{front}/z_{rear}$  was also equal to 2. As a result,  $z_{front}$  was equal to 1.471 m,  $z_{rear}$  was equal to 2.942 m, and  $r$  was equal to 0.736 m. Figure 5 illustrates a diagram of the finalized envelope geometry.

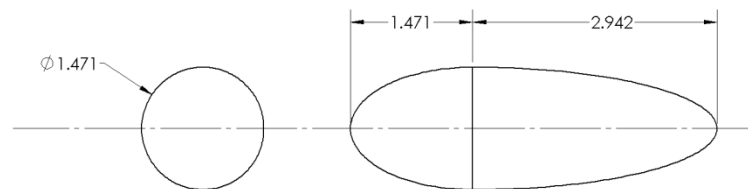


**Figure 5: Diagram of Envelope Geometry**  
**Note: All dimensions are in meters**



### 3.2.2 Aerodynamic Analysis

Using the drag analysis MATLAB script, the drag coefficient of the envelope was 0.035, and the drag force acting on the airship was 3 N.  $\rho_a$ , the density of the ambient air, was selected to be  $1.225 \text{ kg/m}^3$ , and  $\mu_a$ , the viscosity of the ambient air was chosen to be  $1.802 \times 10^{-5}$ . The density and viscosity values are of air at 288 K.  $v_a$  was chosen as 5 m/s, which is the maximum airspeed listed in the design objectives.

### 3.2.3 Stress Analysis

In order to determine the envelope skin material and thickness, methods 1 and 2 were used to determine the membrane stresses. The airship velocity was estimated to be 5.00 m/s and the skin thickness was 0.0001016m. After applying the first method of membrane stress analysis, it was discovered that the maximum bending moments and membranes stresses were relatively small. The maximum bending stress was 2.77 N·m. The maximum longitudinal and hoop stresses were 46.9 kPa and 94.8 kPa, respectively. These values are much lower than the yield strength of the selected material, very low density polyethylene, which is 6.9 MPa. From this program it was also determined that the minimum required pressure,  $p_{min}$ , was 8.73 Pa. Recognizing that the airship will most likely be over pressured, the actual pressure was estimated to be 50% greater, 13.10 Pa.

For the second method of stress analysis, the same skin thickness was used. In addition, the superpressure calculated during the first method was applied. A plot of the longitudinal and hoop stresses along the length of the envelope is printed as Figure 6.

From the MATLAB script using the Burgess method, the maximum longitudinal stress was 37.8 kPa and the maximum hoop stress was 58.1 kPa. Note that the discontinuity in  $\sigma_H$  is a result of the change in the longitudinal radius of curvature at the cross-section of maximum radius. The maximum stresses calculated using the first method are noticeably higher than those in the second. Nevertheless, the maximum membrane stresses in each envelope are within the

same order of magnitude. Because both methods are based upon empirical formulas, these results serve to verify each other to a reasonable level of accuracy. Moreover, the results illustrate that the polyethylene envelope skin will not exceed its yield strength. The thickness of the envelope will not be limited by the stresses, but by its ability to be handled effectively by those constructing the envelope.

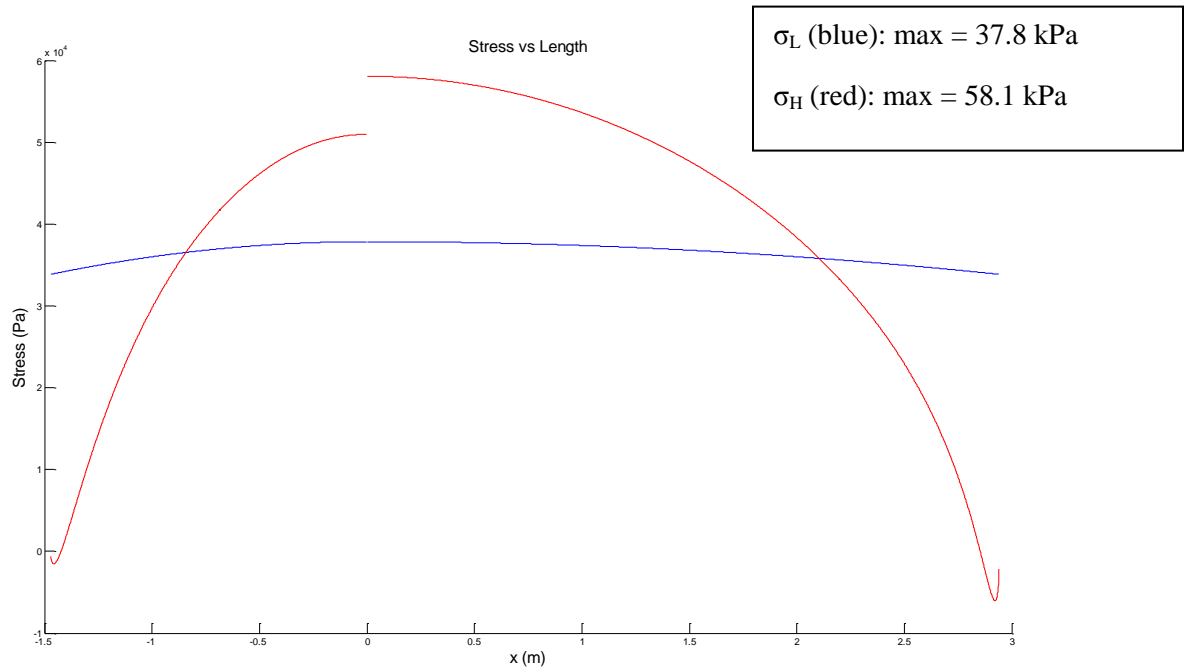


**Figure 6: Stress Distribution of Envelop using Burgess Method**

### ***3.2.4 Envelope Fabrication Methodology***

The airship envelope was made of two .004 in thick polyethylene sheets called gores. The polyethylene material is typically used as a gas and/or fluid barrier when houses are being painted and can be purchased at any home improvement store. A schematic which illustrates the shape of the gores is printed as Figure 7.



**Figure 7: Envelope Gore**

In order to create gores of the appropriate shape, the following analysis was used. As seen in Equation 25, the height of a gore,  $y_g$ , at any given longitudinal cross section is equal to the circumference of the envelope,  $c$ , at that cross section divided by the number of gores,  $n = 2$ .

$$y_g = \frac{c}{n} = \frac{2\pi r}{n} \quad (25)$$

Recognizing that the silhouette of the envelope is two half ellipses, Equation 26 can be used to solve for the radius at each longitudinal cross section. In the equation,  $x$  is the distance of a cross section from the ellipses center;  $r$  is the height from the centerline to the edge at that cross section,  $b$  is the maximum radius, and  $a$  is  $\frac{1}{2}$  the ellipse's maximum length.

$$\frac{x^2}{a^2} + \frac{r^2}{b^2} = 1 \quad \rightarrow \quad r = \sqrt{b^2 \left(1 - \frac{x^2}{a^2}\right)} \quad (26)$$

The front and rear half ellipses use different values of  $a$ , which correspond to values in Figure 5. Equation 26 was substituted into Equation 25 and is printed as Equation 27. The gore shape was created in SolidWorks by using the equation driven curve function to plot  $y_g$ .

$$y_g = \frac{2\pi}{n} \sqrt{b^2 \left(1 - \frac{x^2}{a^2}\right)} \quad (27)$$

The two sheets were bonded using a combination of heat and adhesives. One of the two sheets had an additional inch of material around its entire parameter. The small sheet was then placed on top of the larger sheet. Then the extra inch of material on the larger sheet was folded around the smaller sheet. The sheets were held in place using scotch tape. Then the edges of the

two sheets were ironed together using a clothes iron turned on to the wool setting. The pieces of scotch tape were removed before the iron would pass over them. Between the polyethylene sheeting and the lab floor were Teflon sheets that are typically used for cookie pan liners. The Teflon prevented the polyethylene from adhering to the lab floor. Once the sheets were ironed together, the seam between them was covered using a strongly adhesive 3M number 396 super bond tape. This tape is used to adhere polyethylene barrel liners.

To make filling the envelope with helium simple, a rear wheel tractor tube valve was used. An image of this valve is printed below as Figure 8.



**Figure 8: Envelope Valve**

In order to attach airship components to the envelope, polyethylene strips were to be cut out and taped to the envelope where needed. Then grommets could be pushed through the strips. Fishing line could be fed through the grommets to connect airship components.

### ***3.2.5 Lift Analysis***

Using the default air properties from the static lift MATLAB script, the airship's buoyancy was 6.1 kg, which is 60 N. After accounting for the mass of the helium and the envelop skin, the airship's lift was reduced to 3.6 kg which is 35 N. The temperature of the gases was estimated to be 288 K.

## 3.3 Propulsion and Navigation

### *3.3.1 Introduction to Propulsion and Navigation System*

A schematic that outlines the propulsion and navigation circuit is illustrated in Figure 9.

Due to time and budget constraints, the system presented in this report does not include the components for autonomous flight. However, the system is designed in a manner that makes the integration of autonomous controls possible without re-designing the components presented.

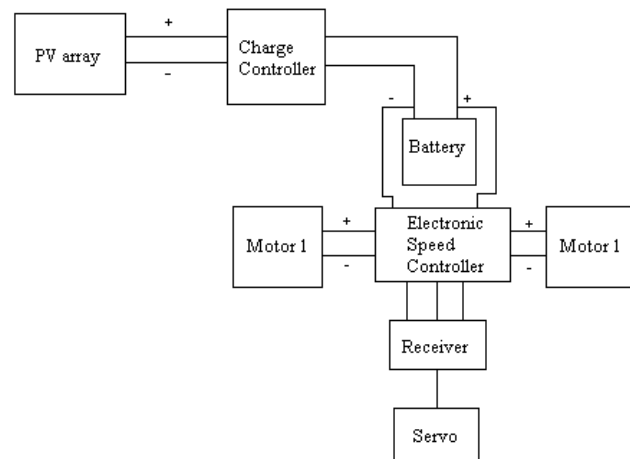


**Figure 9: Schematic of Propulsion and Navigation System**  
**Note: Does Not Include Autonomous Navigation Components**

### *3.3.2 Motor and Ducted Fans*

For propulsion, two six-blade electric ducted fan assemblies are used. An image of one such assembly is printed as Figure 10. Brushed motors are used for two primary reasons. First, they are more affordable than brushless motors. Second, the electronic speed controller used in the system cannot interface with brushless motors.



**Figure 10: Electric Ducted Fan Assembly**

The primary properties of each motor and ducted fan assembly are listed within Table 1. The combined thrust of the two fans is approximately 0.720 kg which is equal to 7.06. N. Using the MATLAB script for aerodynamic drag, it was estimated that the airship should have a maximum velocity of approximately 8 m/s.

Mass, $m_{DF}$ (kg)	0.118
Housing Diameter, $D$ (m)	0.070
Voltage, $V$ (V)	12
Current, $I$ (A)	11
Power, $P$ (W)	132
Rotational Speed $\omega$ , (RPM)	24500
Thrust, $F$ (kg)	0.360
Efficiency (g/W)	2.727

**Table 1: Properties of Single Motor and Ducted Fan Unit ("Watt electric ducted," 2011)**

Ducted fans were chosen instead of propellers because they are more efficient. This allows the ducted fans to have a significantly smaller diameter; thus, the fans and the rest of the airship car can be placed closer to the bottom of the envelope. Minimizing the height of the car reduces its contribution to the airship's aerodynamic drag.

### ***3.3.3 Speed Controller***

Instead of using control surfaces, such as rudders and elevators, the airship was steered by running the motors at different speeds and/or directions. To see a basic schematic of the airship's navigation strategy refer to Figure 11.

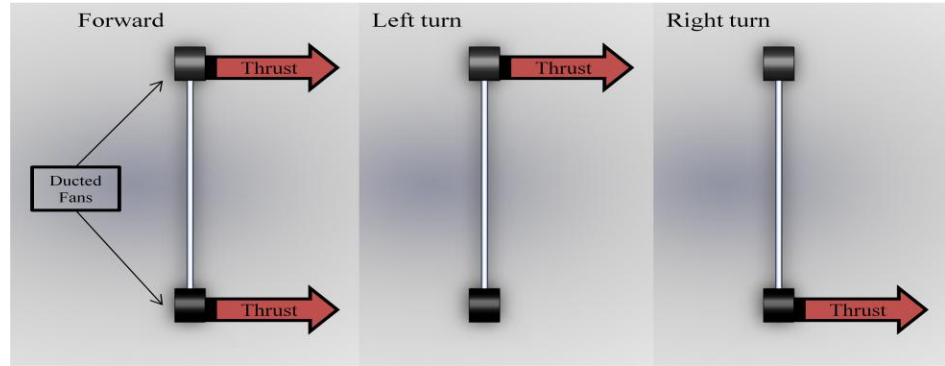


**Figure 11: Simplified Version of Airship Navigation Strategy**

To effectively regulate the motor velocities a Sabertooth dual 12A motor driver was used. This device was chosen because it was specifically designed for radio controlled applications; it is often used in “tank style” robots. In addition, the controller was chosen because it is the smallest commercially available which can sufficiently supply the current needed by the thrusters. Furthermore, the speed controller has an operational setting specifically designed for interfacing with microcontrollers such as Arduino. The device has a mass of 0.060 kg and has the dimensions of 0.059 x 0.075 x 0.017 m. It can continuously supply up to 12 A to each motor (“Sabertooth dual 12a,” 2011). The speed controller’s navigation strategy is significantly more complicated than that illustrated in Figure 11. When the airship is turning, both motors are rotating, albeit, at different speeds. For zero radius turns, the Sabertooth motor driver allows the motors to turn in opposite directions. A picture of the speed controller can be seen as Figure 12.

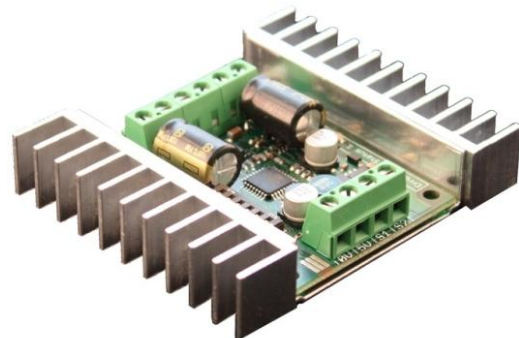


**Figure 12: Sabertooth 2 x 12 A Motor Driver (“Sabertooth dual 12a,” 2011)**

### 3.3.4 Servo

Instead of using elevators, the altitude of the airship is changed by rotating the motors. This is illustrated by Figure 13.

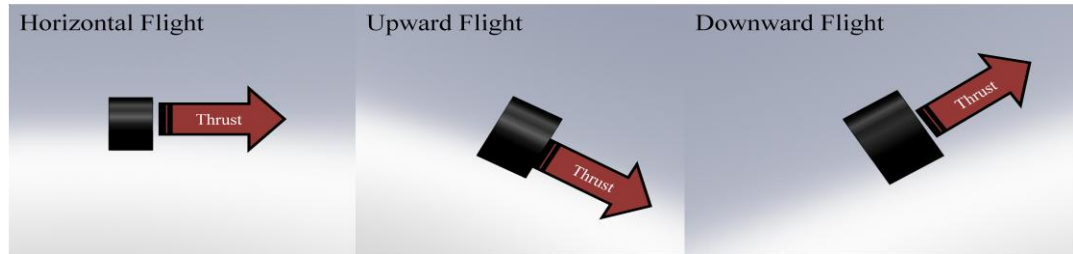


Figure 13: Airship Elevation Control

The motors are rotated through the use of a Futaba S 3305 rotary servo. At 4.8V the servo can supply a torque of 0.697 N·m and a maximum angular velocity of 5.03 rad/s. It has a mass of 0.047 kg ("Futaba s3005 standard," 2004).

### 3.3.5 Receiver and Transmitter

A Futaba R124 H, 27 MHz receiver and a Futaba 4GWD transmitter were used. Although typically used for land based vehicles, this system has a sufficient range and number of channels. It has four channels and has a maximum range of 650 ft. The first channel is connected to the Sabertooth speed controller's S1 port to control the airship's forward and backward motion. The second channel is connected to the speed controllers S2 port and will control the vehicle's turning. The third channel is connected to the servo for controlling the airship's elevation. The fourth channel will remain idle.

### 3.3.6 Photovoltaic Cells

Electricity is generated through the use of 56, 0.0794 m x 0.794 m polycrystalline solar cells. To obtain the average open circuit voltage of the cells, six were selected at random and their open circuit voltages were measured during a period of high solar radiation. The average voltage was  $0.561 \pm 0.008$  V. Under peak solar radiation the cells have a maximum current of



approximately 2A. Two sets of 27 cells in are wired into series. Then these two sets were wired into parallel.

Polycrystalline cells were chosen because they represented a compromise between cost and efficiency. The cells were lighter, more efficient, and cheaper than thin fill cells. These cells are nearly as efficient as single crystal cells; however, they were much more affordable. Because these cells are brittle and will not conform to the envelope surface, it was necessary to attach them to a rigid surface. The mounting surface for the cells will be discussed in Section 3.4.1.

### ***3.3.7 Battery and Charge Controller***

A 6.4 Ah 11.1V, lithium polymer battery produced by Venom Group International for RC car applications is utilized. Having a mass of .499 kg, the battery has a high specific energy, 142 Wh/kg. The battery is capable of burst discharge rates of 192 A and continuous discharge rates of 128 A ("20c 3s 6400mah," 2011). As a result, the battery is able to supply sufficient current to both motors at peak thrust levels. In addition, the battery has minimum discharge voltage of 9V and a maximum charge voltage of 12.6V

Lithium polymer batteries must follow a specific charging regimen and are easily damaged if charged incorrectly. Most photovoltaic systems are designed to use lead acid batteries; consequently, there are very few solar charge controllers commercially available that are designed for LiPo batteries. As a result, it was necessary to order a custom 5A charge controller from Solar Converters Inc. Upon request, PT 12/24-5 charge controller was modified to have a nominal set voltage of 11.1V. The battery's load will be cut off if the battery's voltage goes below 9V. Similarly, charging will cease when the battery reaches its maximum design voltage of 12.6 V.

### 3.3.8 Summary of Propulsion and Navigation Systems

Table 2 provides a summary of all major propulsion system components. In Table 2, component masses and maximum power generation/consumption values are provided. For a more detailed diagram of the propulsion and navigation system circuitry, refer to Appendix 6.2.

	Component	Per Unit		Number of Units	All Units	
		Mass (kg)	Electrical Consumption (W)		Mass (kg)	Electrical Consumption (W)
1	EDF Fan for 400 size motor	0.118	132	2	0.236	264
2	Sabertooth 12 RC Dual Motor Speed Controller	0.043	Not Available	1	0.043	Not Available
3	3.125" x 3.125" PV cell	0.003	-1	56	0.159	-56
4	Solar Converters: 12 V, 5 A Charge Controller	0.227	0.24	1	0.227	0.24
5	Futaba R124H 4-Channel AM Receiver 27MHz	0.015	Not Available	1	0.015	Not Available
6	Futaba S3305 Analogue Servo	0.047	9.6	1	0.047	9.6
7	Venom 6400 Ah 11.1v R/C Car LiPO battery	0.499	0	1	0.499	0
	TOTAL	0.952	140.84		1.226	217.84

**Table 2: Summary of Mass and Power Properties of Electrical Components**

**NOTE: All power generation/usage numbers are maximum instantaneous values. All power consumption properties are supplier provided.**

Table 2 illustrates that most of the airship's power consumed is on behalf of the two fan motors. Because the motors will only be used intermittently, power usage models estimate them to consume a combined 88W. It is assumed that the only energy used by the motors will be to keep the airship stationary. Since the airship will only be used at low wind speeds, the air velocity was chosen to be 2.5 m/s. As a sanity check, this value is about two thirds of the average wind speed in Schenectady in June, 3.71 m/s ("Wind- average wind," 2008). The maximum velocity of the airship was conservatively estimated to be 7.5 m/s.

$$\bar{P}_{motor} = \frac{v_a}{v_{max}} [P_{motor}]_{max} = \frac{2.5 \text{ m/s}}{7.5 \text{ m/s}} (264 \text{ W}) = 88 \text{ W}$$

## **3.4 Rigid Structural Components**

### ***3.4.1 PV Cell Backing***

Because polycrystalline photovoltaic cells are extremely brittle, it was necessary to connect them to a rigid structure made of 1/4" balsa wood. Figure 14 illustrates a CAD rendering of the structure on the envelope, and a photograph of the fabricated assembly.

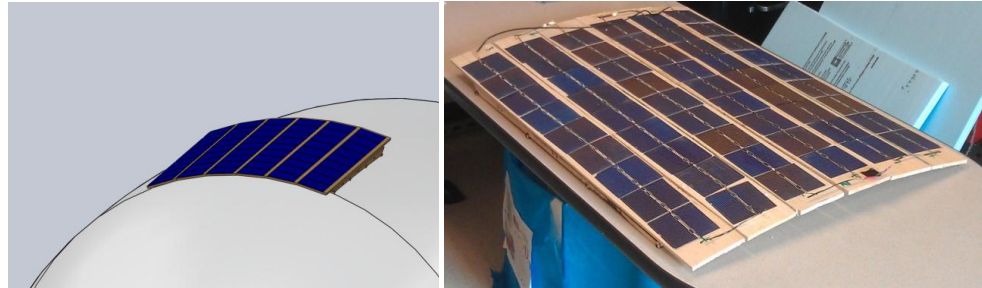


**Figure 14: PV Cell Backing**

The top of the panel is made of six planks which run in the longitudinal direction of the airship. The front and rear of the boards are at the same radial distance from the envelope's centerline. Under the planks is a skeleton made of longitudinal and radial beams designed to fit the contour of the airship's envelope. All parts were created within SolidWorks. The longitudinal curves were created using the SolidWorks equation driven curve feature. Small holes were included along the outer perimeter of the substructure. These make it possible to tie the PV panel to the envelope with fishing line.

The upper planks were cut using a band saw. The substructure pieces were cut using a laser cutter. All components were adhered using Testors Cement for Metal and Wood Models. Engineering drawings of all subcomponents are attached as section 6.3 of the Appendix. A picture of the substructure is illustrated as Figure 15.

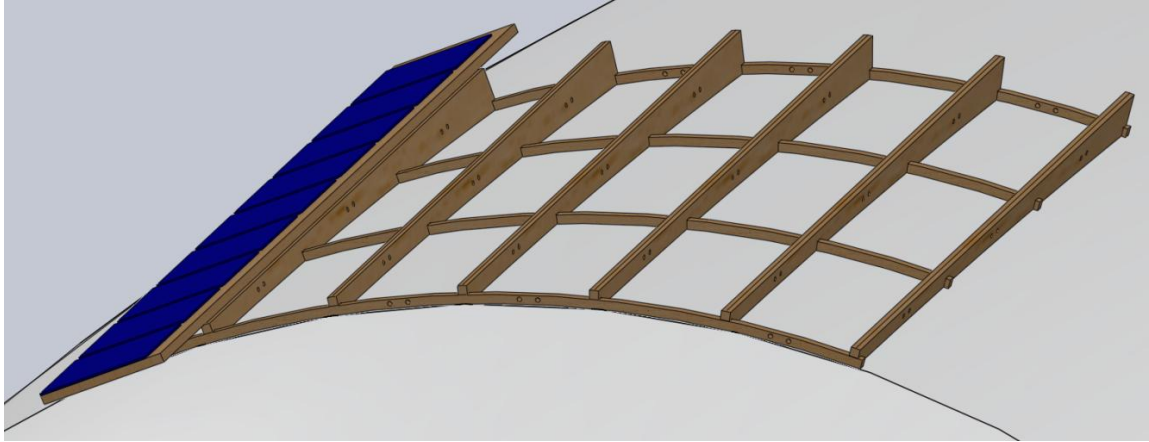


**Figure 15: PV Panel Substructure**

### **3.4.2 Fins**

In order to increase the stability of the airship, fins were created to attach to the airship envelop. Figure 16, illustrates the fins as part of a SolidWorks assembly. Figure 17 illustrates a fabricated fin next to a SolidWorks model.

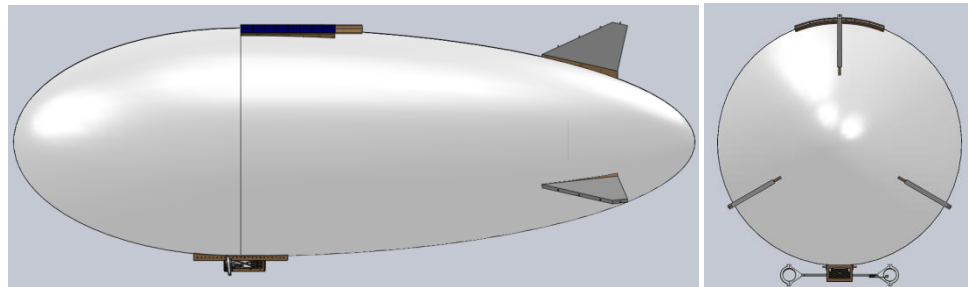


**Figure 16: Fins as Part of Full Airship CAD Assembly**

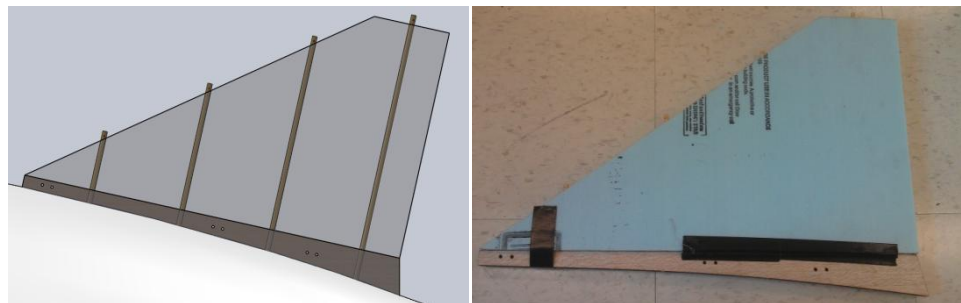


**Figure 17: Fabricated Fin and Transparent View**

The fins are made of 1" thick Dow Styrofoam Brand insulation. The fin bases are made of two pieces of 1/4" balsawood sheeting that were laminated together. They were cut out using a laser cutter. 1/4" diameter holes were drilled completely through the fin and the base. Holes were

included in the fin bases so that they could be attached to the envelope using fishing line. As Figure 15 illustrates,  $\frac{1}{4}$ " dowels were inserted into both the fin and the base for added strength. Testors Cement for Metal and Wood Models was used to glue the dowels into the base, and tape was used to attach the fin to the base.  $\frac{1}{16}$ " holes were drilled through the top of each dowel. To keep the fins upright, fishing line will be run from the top of the dowels to points on the envelope on both sides of each fin. Engineering Drawings of all subcomponents are attached as section 6.3 of the Appendix.

### 3.4.3 Gondola

Like the PV base and the fins, the gondola was constructed primarily out of  $\frac{1}{4}$ " balsa wood sheeting. Images of the gondola are illustrated as Figure 18. The four gondola walls were fabricated using a laser cutter. All other components were created using a band saw and drill press. The top two pieces of the gondola, as seen in Figure 18, are tightly fixed to the envelope through the use of fishing line. The rest of the gondola is attached to these pieces by three  $\frac{1}{4}$ " aluminum rods. The ends of the rods are threaded with wing nuts at either end. The gondola can easily be removed by unscrewing the wing nuts and pulling the rods out. Once it is removed from the airship, gondola's wall can be removed so that the electrical components are easily accessible. The walls are detached by removing twelve 8-32 bolts. Drawings of all subcomponents are attached as section 6.3 of the Appendix.



**Figure 18: Airship Gondola: CAD Rendering (left), Fabricated Assembly (Right)**

When designing an airship, it is necessary for the center of mass of the airship to be directly below the airship's center of gravity. If the center of gravity is above the center of buoyancy, the airship will roll over. If the center of gravity is below the center of buoyancy, but at another position along the airship's longitudinal axis, the airship will have a tendency to go into either a forward or backward dive.

The following procedure was used to determine the position of the gondola:

First: The center of mass of the entire airship without the gondola was calculated using the mass properties function in SolidWorks. This model included the helium inside the envelope. All components were modeled to have the correct density, and the net weight of the assembly was reported as 3.799 kg.

Second: The center of mass of the SolidWorks helium piece inside the envelope was calculated. It was estimated that this position was the center of lift due to Archimedes's principle. Also, it was estimated that the lift was 6.1 kg, 60 N, the weight of the air displaced by the airship envelope.

Third: Once the gondola was created its mass was found using the mass properties function. The weight of all electrical components was then added to this value.

Fourth: A free body diagram was used to determine where the gondola should be positioned. The free body diagram is printed as Figure 19. In the Figure,  $x$  is the distance from the gondola weight to the center of buoyancy;  $F_b$  is the Archimedes's principle lift;  $F_g$  is the gondola weight; and  $F_w$  is the weight of all other components.  $x$  was solved for using Equation 25.

$$\sum M_o = 0 = xF_g + x_bF_b + x_wF_w \quad (25)$$

In Equation 25,  $x_b$  is the distance from the plane of maximum radius to the buoyancy force;  $x_w$  is the distance from the plane of maximum radius to the center of gravity of all non-gondola components; and  $M_O$  is the sum of the moments about the plane of maximum radius. It was calculated that  $x$  is equal to .501m

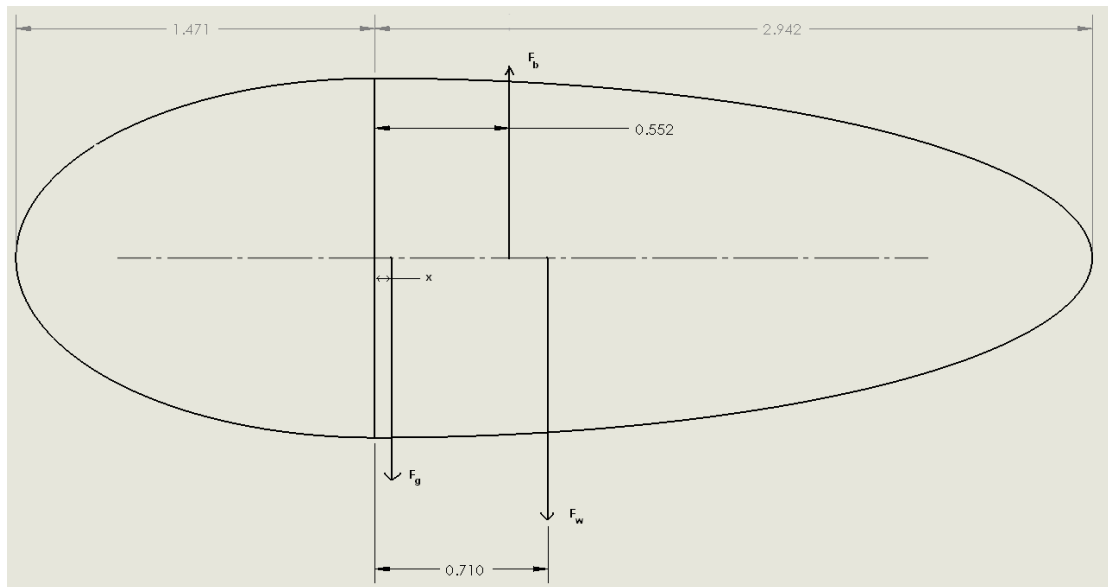


**Figure 19: Free Body Diagram to Calculate Gondola Position**

There are many factors which could change the actual desired gondola position from that which was calculated. Three of these are:

1. The actual envelope shape will not be perfectly formed.
2. The weight of the balsa components was based on a density provided by SolidWorks, which may deviate from the actual value.
3. Analysis did not include the weight of minor components, such as wires, fasteners, and glue.

Due to these variables, it was decided to make the gondola's position variable. The piece which attaches directly to the envelope has 23 equally spaced holes, as seen in Figure 20. This allows the gondola to be adjusted 6.5" in either direction away from its calculated position

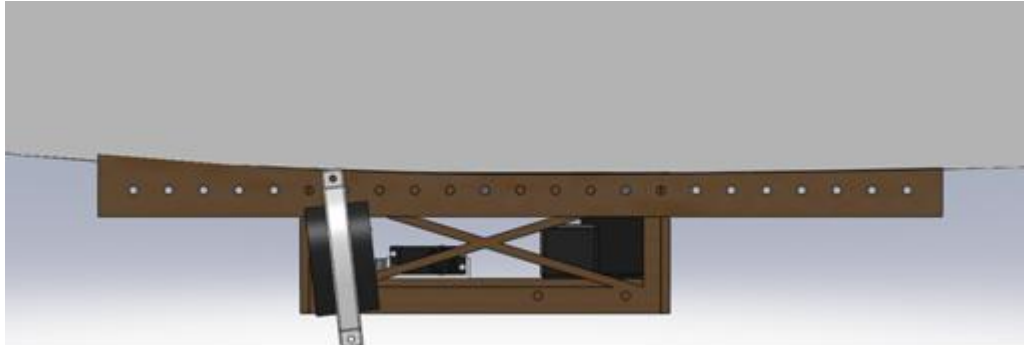


**Figure 20: Gondola Position Adjustor**

### **3.5 Fan and Axel Assembly**

A schematic which illustrates the ducted fan rotation assembly is represented as Figure 21. Engineering drawings of all components in the Fan and Axel Assembly are attached in section 6.3 of the Appendix. As Figure 21 illustrates, the two ducted fans are linked via an aluminum rod. The rod illustrated is 18" long. If the motors do not produce sufficient moments to rotate the airship, an interchangeable 24" long rod was fabricated. The fans are fixed to the aluminum rod by ABS plastic clamps that were fabricated using a rapid prototyping machine. The connecting rod is attached to the gondola base by two ABS fixtures that were rapid prototyped. A thin layer of light weight grease was placed between the brackets and the rod to reduce friction.



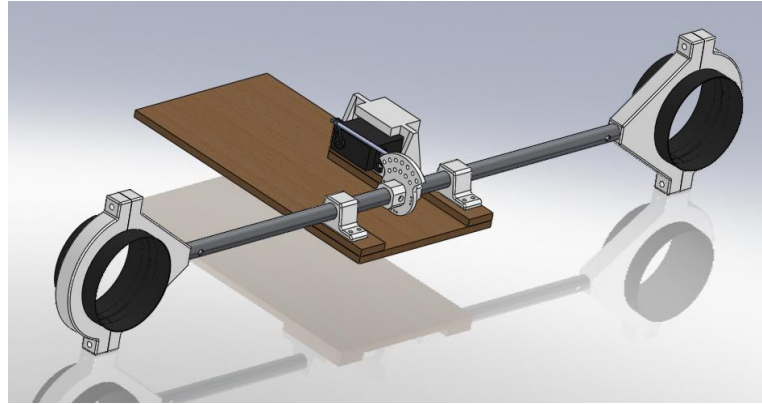


**Figure 21: Ducted Fan Assembly**

The Futaba S3305 servo rotates the ducted fans through the use of a four bar linkage mechanism. A photograph of the mechanism is represented as Figure 22.

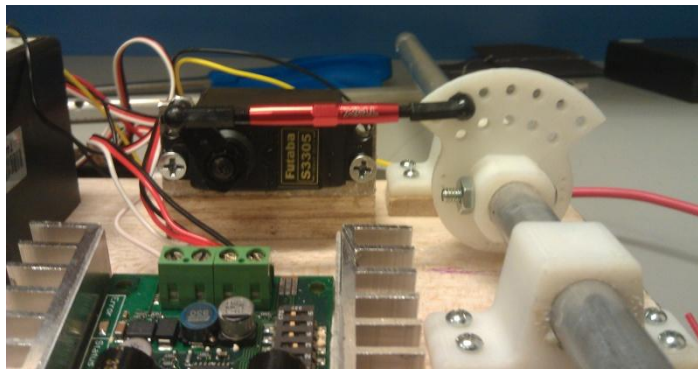


**Figure 22: Four Bar Linkage Mechanism**

The geometry of the mechanism was developed using a SolidWorks model. The mechanism was designed so that the motors would rotate forward and backwards an equal amount. Due to possible fabrication and assembly errors it was decided to make two of the four linkage bars adjustable. The ends of the coupler link are threaded into its center piece. The coupler's length can be adjusted by extracting or retracting its ends. The link that is attached to the ducted fan axel has many attachment points for adjustment.

## **4 Testing and Results**

### **4.1 Envelope**

Several small scale envelopes were fabricated and tested using air as the internal gas. Unlike the envelope fabrication methodology outline in the report, initial attempts used three longitudinal gore sections. The first attempt used only heat to combine the seams. The envelope leaked considerably and it was not possible for it to be fully inflated. On the second envelope attempt, 3M #396 super bond tape was placed over the seams. It was then possible to fully inflate the airship. However, there was a considerable amount of leaking that occurred at the ends of the envelope and it deflated within a few minutes. Problems arose because it was difficult to get the three sheets to join at a single point.

It was attempted to correct the problem by attaching end patches to the envelope. Instead of meeting at a single point, the gores would attach to a 6" diameter circular sheet at each end. During this trial, both heat and tape were used to seal the seams. The envelope still leaked considerably, albeit, at a slightly decreased rate.

At this point, the three gore strategy was abandoned for the two gore strategy outlined within the report. Although using two gores would cause the envelope shape to form less accurately, it alleviated the problem of having to attach three plastic sheets at a single point. This method provided the best results. It was possible to fully inflate the envelope. There were no major leaks that were felt, seen or heard. An image of this small scale test is illustrated as Figure 23. Nevertheless, the envelope still slowly leaked. It completely lost its internal air over the course of approximately eight hours.



**Figure 23: Small Scale Envelope Test**  
**Note: Dimensions of small scale envelope were not proportional to those of full scale design**

The results of the final small scale test were considered unsatisfactory in order to advance to full scale fabrication. Under compressive forces the envelope deflated even more rapidly. Furthermore, the envelope would leak faster if filled with helium. In order to address issue of deflation, the gas retention of the polyethylene sheeting should be further analyzed to ensure that it is satisfactory. In addition, alternative methods of sealing polyethylene sheets should be researched. Possible useful contacts include parade balloon manufacturers and the creators of small scale blimps for sporting events.

## **4.2 Propulsion and Power Generation**

### ***4.2.1 Propulsion and Navigation***

In its current state, the propulsion system functions adequately. Using the R/C transmitter, an operator can easily signal the ducted fans to provide forward or backward thrust. The operator can also signal the fans to provide thrust in opposite directions for turning. In addition, the servo pitches the motors up and down in order to provide positive and negative lift.

With both motors at full thrust the propulsion system draws approximately 254 W. This value was calculated by placing a precision 0.10  $\Omega$  resistor between the positive terminal of the battery and its appropriate connection port on the Sabertooth speed controller. The charging system was disconnected. The motors were run at full thrust, and simultaneously the voltage was measured across the resistor using a voltmeter. The voltage across the resistor was 2.06V. Using Ohms law it was calculated that the system was drawing a current,  $I$ , of 20.6 A. Then the voltage across the battery,  $V$ , was measured at 12.34 V while the motors were at full thrust. Equation 26 was used to calculate the power,  $P$ , drawn by the system.

$$P = IV \quad (26)$$

Further work can be done to optimize the propulsion system. In the design process it was expected that the Futaba S3305 servo would have an operational 180° range of motion. However, in use the servo has approximately a 90° range of motion. As a result, the ducted fans can only

rotate approximately  $60^\circ$  ( $30^\circ$  forwards or backwards). For improved navigation, the linkage geometry should be reevaluated to provide a greater rotational range of motion. Another option which would provide a greater range of motion is to use a continuous rotation servo with a pulley placed on its output shaft. Then a taut rubber band would be placed between the pulley and the motor connect rod.

#### ***4.2.2 Photovoltaic Charging System***

On Monday June 6<sup>th</sup>, the PV module was brought outside for basic testing. At 3:30 PM under clear skies PV module had an open circuit voltage of 14.5 V. The module also had a short circuit current of 3.25 A.

The follow procedure was used to test if the system charges the battery. The electrical system was turned on in a laboratory environment with the PV cells detached. The motors were run until the battery voltage had dropped from 12.6 V to 12.29 V. Then a constant voltage electrical power supply was wired to the charge controller in place of the PV module. It was found that the charge controller would not draw a current unless the power supply had a voltage of at least 15.2V. Then the power supply used to charge the battery while providing a current of 1.64 A at 15.5V. Table 3 was made of the batteries voltage over time. Being that the battery's voltage steadily increased over time it was deemed that the battery was charging.

Time (min)	Voltage (V)
0	12.29
5	12.39
10	12.43
15	12.47
20	12.59

**Table 3: Voltage of Battery over Time While Being Charged**

However, it was noted that the battery's voltage continued to increase beyond 12.6 V. When the batteries voltage reached 12.9 V it was interpreted that the charge controller was not correctly limiting current to the battery, and the charging process was stopped. The supplier was contacted and reported that the charge controller was set for a nominal 12 V battery. The supplier stated that there may be a trim POT in the unit that can be adjusted to 11.1 V. The charge controller must be taken apart to see if it can be adjusted. Once adjusted it must be seen if it will draw a current with an input voltage of approximately 14 V. If it does not, additional solar cells must be added. If it is undesirable to re-fabricate the PV module, these cells can be added to the airship's fins. The fins should be attached in an alternate geometry so that they are not blocked from the sun.

### **4.3 Weight Analysis**

The masses of all envelope attachments were measured using an AND FG-60K digital scale. The mass of the gondola was 1.70 kg; the mass of the PV module was .78 kg; and combine the mass of the three fins was .36kg. The sum of these values is equal to 2.84 kg. As calculated by the MATLAB script, the airship envelope should be able to lift a maximum mass of 3.6 kg. In order, to make the airship neutrally buoyant, the envelope's internal helium can be diluted with air. Another option is to place grommets below the airship's center of mass and attach ballasts as necessary.

## **5 References**

*20c 3s 6400mah 11.1v r/c car lipo - uni.* (2011). Retrieved from <http://www.venom-group.com/itemdesc.asp?ic=15009>

Burgess, C.P. (2004). *Airship design*. Honolulu, HI: University Press of the Pacific.

*Futaba S3305 High-Torque Standard Servo w/Metal Gears* (2004, October 29). Retrieved from <http://www.gpdealera.com/cgi-bin/wgainf100p.pgm?I=FUTM0045>

Gillett, J.D., & Khoury, G.A. (2004). *Airship technology*. New York, NY: Cambridge University Press.

*Mylar polyester film; physical-thermal properties.* (2003). Hopewell, VA: Dupont Teijin Films.

Pringle, D. (2002, March). *5 amp charge controller*. Retrieved from [http://www.solarconverters.com/product\\_frame.html](http://www.solarconverters.com/product_frame.html)

*Sabertooth dual 12a motor driver.* (2011). Retrieved from <http://www.dimensionengineering.com/Sabertooth2X12.htm>

*Watt electric ducted fan.* (2011). Retrieved from [http://www.ductedfans.com/impellers\\_watt\\_fan.html](http://www.ductedfans.com/impellers_watt_fan.html)

*Wind- average wind speed- (mph).* (2008, August 20). Retrieved from <http://lwf.ncdc.noaa.gov/oa/climate/online/ccd/avgwind.html>

## 6 Appendix

### 6.1 Geometry Derivations

Equation 1A below describes the volume of an envelope shape.

$$V = \frac{2}{3}\pi r \left[ (z_{front})^2 + (z_{rear})^2 \right] \quad (1A)$$

As seen below Equation 1A was rearranged to determine the value of the maximum radius,  $r$ , within the MATLAB script.

$$z_{front} = r c_1 \quad (2A)$$

$$z_{rear} = z_{front} c_2 = r c_1 c_2 \quad (3A)$$

$$V = \frac{2}{3}\pi [c_1 + c_1 c_2] r^3 \quad (4A)$$

$$r = \left[ \frac{3V}{2\pi c_1 + c_2 c_3} \right]^{\frac{1}{3}} \quad (5A)$$

Once the radius is calculated,  $z_{front}$  and  $z_{rear}$  are determined by the script using equations 2A and 3A respectively.

The surface area of the envelope,  $A$ , was calculated using Equation 4. The derivation for Equation 4 is below.

$$A = \pi \left( 2(r^2) + \frac{r(z_{front})(\alpha_{front})}{\sin \alpha_{front}} + \frac{r(z_{rear})(\alpha_{rear})}{\sin \alpha_{rear}} \right) \quad (4)$$

$$\text{where: } \alpha_{front} = \cos^{-1} \left( \frac{r}{z_{front}} \right)$$

$$\alpha_{rear} = \cos^{-1}\left(\frac{r}{z_{rear}}\right)$$

Equation 6A is used to find the surface area of a prolate spheroid.

$$A = 2\pi\left(r^2 + \frac{rz\alpha}{\sin\alpha}\right) \quad (6A)$$

$$\text{where: } \alpha = \cos^{-1}\frac{r}{z}$$

$$z = \frac{1}{2} \text{ the maximum length of the p}$$

Both the front and rear segments of the envelope are half of a prolate spheroid. Both segments have the same maximum radius,  $r$ . The surface area of the front segment is found using Equation 7A.

$$A = \pi\left(r^2 + \frac{rZ_{front}\alpha_{front}}{\sin\alpha_{front}}\right) \quad (7A)$$

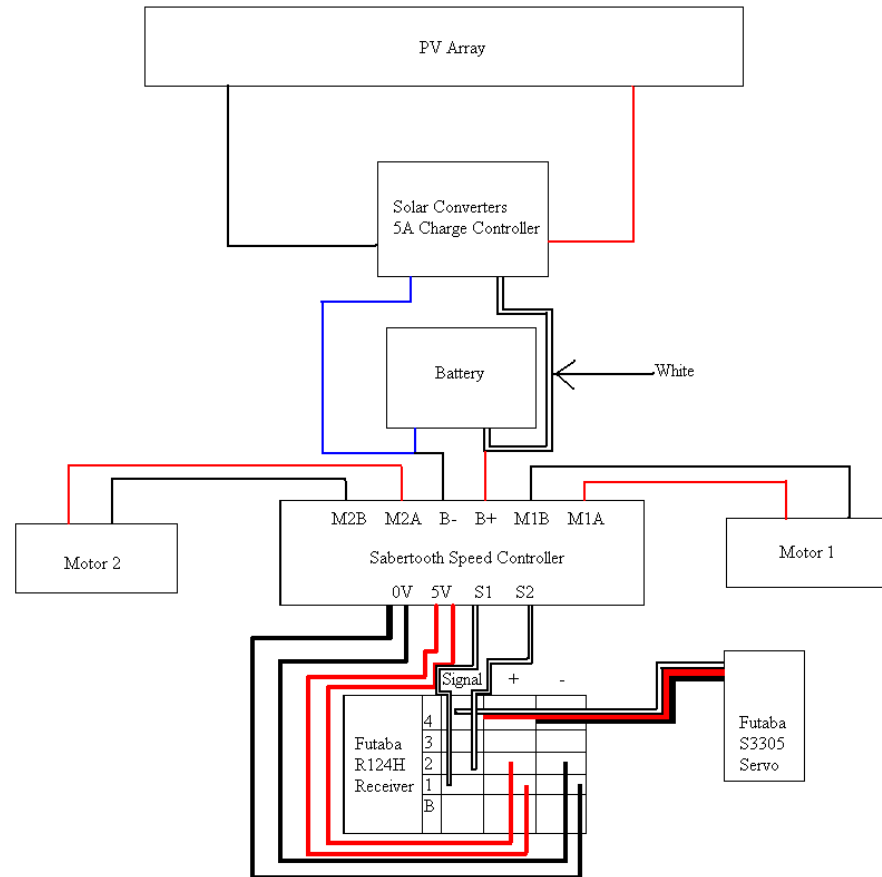
The surface area of the front segment is found using Equation 8A.

$$A = \pi\left(r^2 + \frac{rZ_{rear}\alpha_{rear}}{\sin\alpha_{rear}}\right) \quad (8A)$$

The surface area of the entire airship is the sum of equations 7A and 8A.



## 6.2 Detailed Circuit Diagram



## 6.3 Engineering Drawings